



The Egyptian Journal of Remote Sensing and Space Sciences

journal homepage: www.sciencedirect.com



Research Paper

Investigating land use land cover changes and their effects on land surface temperature and urban heat islands in Sharqiyah Governorate, Egypt

Asmaa Hamed Fahmy*, Mohamed Amin Abdelfatah, Gamal El-Fiky

Construction Eng. & Utilities Department, Faculty of Engineering, Zagazig University, Egypt

ARTICLE INFO

Article history:

Received 1 January 2023

Revised 22 March 2023

Accepted 4 April 2023

Available online 19 April 2023

Keywords:

Urban Heat islands

Land surface temperature

Landsat

Land use land cover

ABSTRACT

The Urban Heat Island (UHI) issue is a result of the undesirable effects of urban growth on the environment, such as temperature rises and landscape changes that cause environmental dangers. Thus, the purpose of this research is to investigate the effect of Land Use Land Cover (LULC) change on Land Surface Temperature (LST) and then study UHI in Sharqiyah from 2001 to 2022 using remote sensing data. This data was collected from the Landsat satellite and Moderate Resolution Imaging Spectroradiometer (MODIS) 11A Thermal sensors. A Mono-Window Algorithm was used on Landsat 8 and 9 data to estimate the LST. To determine the LST and UHI, the thermal band was utilized. LULC maps were created using the Support Vector Machine (SVM) classification technique. To evaluate various LULC indices in the Sharqiyah and find their correlation with LST, the spectral indices Normalized Difference Vegetation Index (NDVI), Normalized Difference Bare Land Index (NDBal), and Normalized Difference Built-up Index (NDBI) were obtained from the processing of multispectral Landsat data. To check data sources, air temperature measurements for Sharqiyah were also acquired. The results show that urban expansion has increased in a noticeable trend. The built-up area increased by 18.9% during the research phase, and the region's mean LST increased within 3.98°C. The UHI threshold temperature increased by 4.27°C. This research is critical for Planning Engineers and environmental scientists to realize LULC variations effects on LST and to suggest suitable political steps to regulate urbanization in Sharqiyah Governorate.

© 2023 National Authority of Remote Sensing & Space Science. Published by Elsevier B.V. This is an open access article under the CC BY-NC-ND license (<http://creativecommons.org/licenses/by-nc-nd/4.0/>).

1. Introduction

One of the main important environmental factors influencing our ecosystems and daily lives is the climate (Hunt et al. 2017). According to the United Nations (2018), by 2050, 68 % of the earth's population will be sensitive to Surface Urban Heat Island (SUHI) due to the fast-increasing trend of Land Surface Temperature (LST). Urbanization and increased industrialization are causing massive Land Use Land Cover (LULC) variations (Mundhe and Jaybhaye 2014), which appear to be the primary causes of rising air temperatures (Al Rakib et al. 2020). The fast change in urban LULC is occurring as the urban population continues to rise (Ramachandra, Bharath, and Gupta 2018). The urban population is rapidly rising as a result of continuous movement from the rural in need of better employment chances (Dutta et al. 2021). The distribution of LULC such as buildings, highways, and green areas in urban regions is strongly related to LST, with each component

possessing its own unique heating and radiation qualities (Bokaei et al. 2016). Changes in urban LULC accelerate climate change because LULC is related to reducing biodiversity and producing the UHI effect (A. Al Kafy et al. 2021a). The reduction in agricultural and water areas is associated with increased absorption of solar radiation, leading to rising LST with harmful effects on climate and human life (Owen, Carlson, and Gillies 1998; Fadhil et al., 2023). The most apparent change in the climate, according to (Jones, Wigley, and Wright 1986), is an increase in air temperature. Overall, the temperature is seen to be higher in urban regions than in the nearby rural ones (Liu et al. 2016). The Urban Heat Island (UHI) effect is the name given to this concept, driven by elevated LST. The UHI phenomenon produced by human activity has led to substantial economic and health difficulties affecting more than half of the world's population, including increased energy usage in summer for cooling, negative impacts on residents' health and air quality, and ecosystem disruption (Fadhil et al., 2023). UHI can significantly impact cities' sustainable development and their surrounding areas (Sharma et al. 2016). Remote sensing has been used to study the effects of UHI in both urban and non-urban areas,

* Corresponding author.

E-mail address: asmaa7amed259@gmail.com (A. Hamed Fahmy).

so many cities around the world have studied UHI using remote sensing (Ward et al. 2016). Remotely sensed data provide the ability to analyze patterns at different time scales, including sub-seasonal ones. Technological progress has enabled the capture of both optical and thermal data using the same sensor platforms, which is valuable for studying urban land cover changes and thermal conditions (Choe and Yom 2020). Moderate-resolution sensors such as Landsat, ASTER, and MODIS are commonly used to assess how land use and land cover alterations affect the thermal environment (Zhang et al. 2021).

Using data from satellites with a medium spatial resolution, such as Landsat Thematic Mapper (TM), Enhanced Thematic Mapper+ (ETM +), Operational Land Imager/Thermal Infrared Sensor (OLI/TIRS), and MODIS, a wide range of research on the SUHI phenomenon is carried out. Thermal wavelength satellite sensors can provide spatially complete and time-synchronized coverage of an urban area; in contrast to static stations and vehicle traversal, real higher and lower temperatures across a city region can be achieved (Johnson et al. 1991), and thermal characteristics inside cities can be discovered. As thermal remote sensing systems advance, UHIs may now be observed from airplane and satellite systems, opening up new options for UHI observation. To recover LST using TM/ETM + data, several techniques have been devised, including the mono-window algorithm (Qin, Karnieli, and Berliner 2001), and the single-channel algorithm (Jimenez-Munoz et al. 2009). Landsat data has also been widely utilized to map LULC and identify changes (Shen et al., 2011). As a result, since the 1970 s, researching LULC changes has been regarded as vital research in the spatial analysis of remote sensing (Lo and Shipman 1990).

Also, since the mid-1990 s, several spectral indices, such as, the Normalized Difference Vegetation Index (NDVI), the Normalized Difference Built-up Index (NDBI), and the Normalized Difference Bare Land Index (NDBal) have been able to be employed for precise and rapid classification from satellite data (Elbeih and El-Zeiny 2018). Several studies have been performed to discover the connection between LULC indices and LST in various ways. LST is rising because of the transformation of vegetated surfaces into impervious areas, according to (Pal and Ziaul 2017). (Ogashawara and Bastos 2012) observed that built-up areas promote urban temperature, whereas vegetation and water bodies give a low LST. According to (Chen et al. 2006), there is a substantial relation between NDBI and LST and an inverse correlation between NDVI and LST.

In Egypt, several types of research were performed to better investigate the UHI and its harmful effects on the environment. (El-Magd, Ismail, and Zanaty 2016) illustrated the use of thermal remote sensing using Landsat time series to identify the intensity and variation of UHIs in Cairo. The ability of remote sensing was evaluated and GIS to assess El-Fayoum governorate LST (El-Zeiny and Effat 2017). While several studies have examined the relationship between LULC changes, UHI, and LST in various urban areas, few studies have investigated these phenomena in Sharqiyah, particularly in conjunction with Numerical Weather Prediction to calculate air temperature. Therefore, the present study aims to address this research gap by employing remote sensing techniques. Specifically, our objectives are to 1) map and evaluate LST and UHI patterns in Sharqiyah using Landsat thermal bands, 2) NDBI, NDBal, and NDVI calculations, and 3) analyze the relationship between LULC changes and LST/UHI variations between 2001,

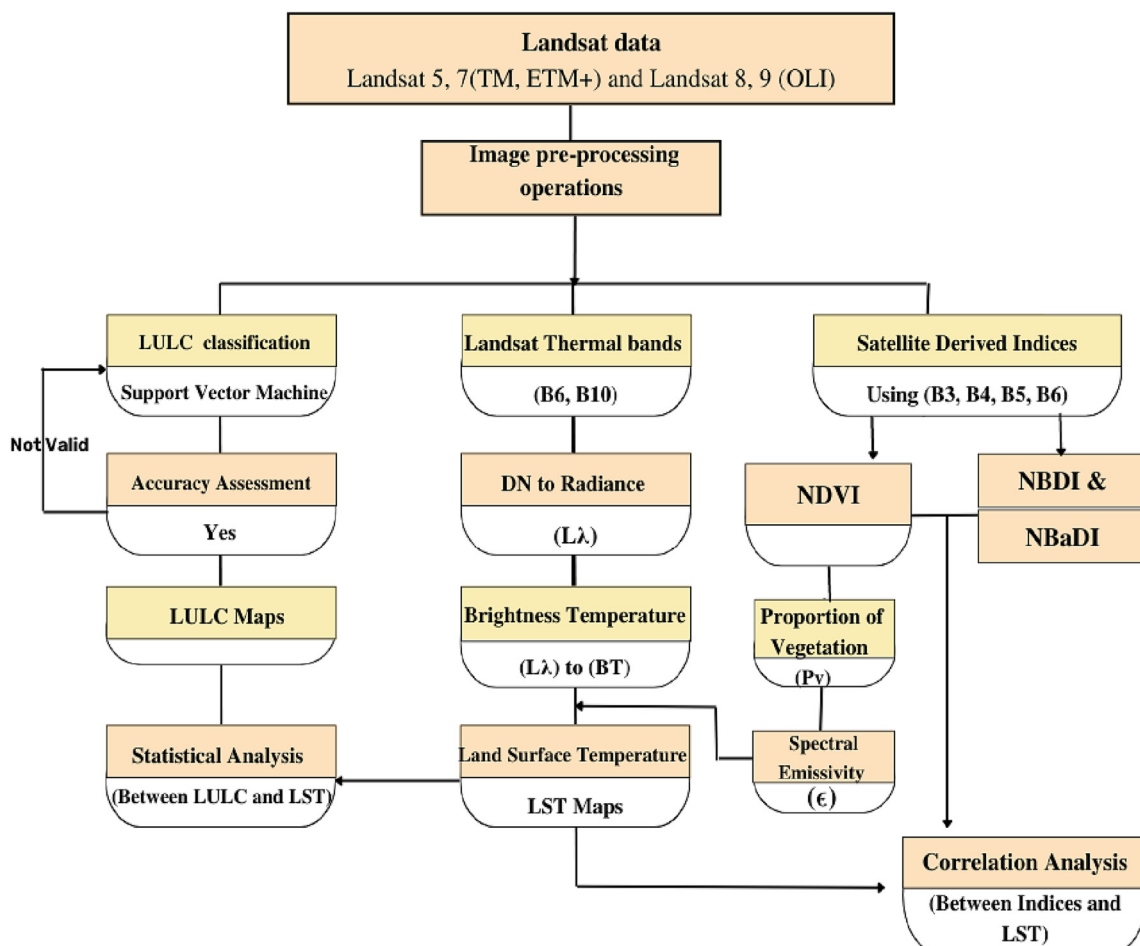


Fig. 1. Flowchart of the methodology of the study.

2011, and 2022, using Landsat TM and OLI data. To satisfy the purpose of the study, the following data and techniques were employed, and represented as a flowchart as shown in Fig. 1.

2. Materials and methods

2.1. Study area

Sharqiyyah Governorate is Egypt's third most popular governorate, covering about 4818 km². Its capital is Zagazig, and the 10th of Ramadan City is one of its largest industrial cities. It is placed in the country's northern region and on the eastern edge of the Nile Delta, between longitudes 31° 15' and 32° 15' E, and latitudes 30° 10' and 31° 5' N, as shown in Fig. 2. On the north, it is bounded by the governorates of Port Said and Dakahlia, on the east by the governorate of Ismailia; on the south by the governorate of Cairo, and on the west by the governorate of Gharbia. Sharqiyyah has rich agriculture and industrial cities. Sharqiyyah grows each day, and the increased population puts a strain on housing and other associated needs. Sharqiyyah has a hot desert climate with high temperatures and low humidity all year round, and very little rain in winter. In summer, temperatures can reach up to 40 °C during the day, and at night, temperatures can drop to 25–30 °C, which may still be uncomfortably warm for some.

2.2. Data sources

In the research, Satellite Landsat imagery TM, ETM+, and OLI/TIRS for each study year (2001, 2011, and 2022) was obtained using the website link (<https://earthexplorer.usgs.gov>), the United States Geological Survey (USGS) (path 176 / row 39). Landsat data was selected due to its advantages, such as high spatial resolution, a longer data archive, and the ability to capture visible and near-infrared spectral bands, but it also has disadvantages, such as lower temporal resolution (Roy et al. 2014). Using MODIS or Sentinel data has advantages such as higher temporal resolution, wider spectral coverage, and free data access, but the lower spatial resolution and less available data archive compared to Landsat are some of its disadvantages (Justice et al. 2002; Van der Werff and

Van der Meer 2016). Dates in each year's summer season were picked to keep a similar seasonal state. Data were also reviewed to ensure that there was no cloud. Landsat 5 was used for 2001 and 2011, Landsat 7 was used for 2012 and 2013, Landsat 8 was used from 2014 to 2021, and Landsat 9 was used for 2022. MODIS imagery was used in 2001 and from 2011 to 2022. European Reanalysis Dataset 5 (ERA5) is the Copernicus Climate Change Service's latest version of The European Centre for Medium-Range Weather Forecasts (ECMWF) atmospheric reanalysis of global climate (Muñoz Sabater 2019). It uses complex modeling and data assimilation technologies to merge enormous volumes of past observations into universal calculations. On a roughly 0.25° × 0.25° worldwide grid, estimates of many air, land, and oceanic climate factors are provided starting in 1979 and possibly going back to 1950.

2.3. LULC classification

The bands of Landsat 8 were combined to create a multi-band image, which was subsequently processed to a resolution of 30 m and mapped to the WGS 84/UTM zone 36 N used ArcGIS software. LULC classification means automatically grouping each of the image's cells into different classes of land cover. Different classification strategies have been used in earlier research to classify satellite imagery cells into numerous LULC classes utilizing multi-temporal Landsat satellite imagery (Rimal et al. 2017). LULC in Sharqiyyah was divided into four categories, namely, vegetation, built-up, bare land, and water bodies, using Support vector machine (SVM) classification techniques (Lee, Hong, and Jung 2017). Based on its high accuracy, the SVM classifier was selected above other supervised classification strategies (A.-A. Kafy et al. 2021). After that, the accuracy of the LULC classification must be evaluated based on how well the photos are classified.

For the accuracy assessment, sample points of Sharqiyyah were chosen using an irregular stratified selection strategy. For all years, several samples were utilized to correlate classified imagery cells with reference points. For each classified image, about 400 earth-points were collected to examine the precision of the LC classifica-

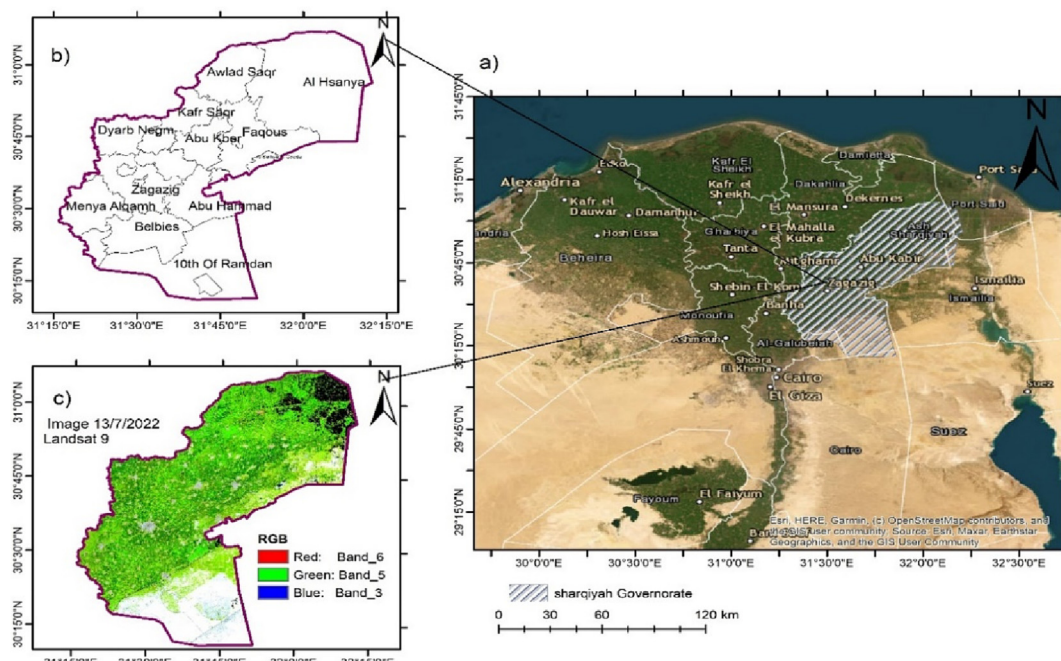


Fig. 2. Study region, a) Location of Sharqiyyah in Egypt. b) Sharqiyyah Governorate. c) Landsat 9 image for Sharqiyyah.

tions. The past Google Earth information was used to get the actual points for the various land cover classes.

So, some statistical strategies were used: user's accuracy (UA), which focuses on earth's reality probability, and producer's accuracy (PA), which focuses on classification fitness. Based on these strategies, the overall accuracy (OA) was estimated. Then it was determined using kappa statistics (K), which is a non-parametric indicator developed to assess the degree of similarity between producer and user values. Past research indicated that the required accuracy rate for LULC classification should be set at 80 % (Rousta et al. 2018).

2.4. Extraction of different LULC indices

NDVI is the most commonly used criterion for detecting vegetation. NDBal was used to determine the amount of bare land on the land surface. NDBI is a further important urban climate indication for ecological observation. These three indices can be applied to categorize different types of LULC (Table 1).

2.5. Land surface temperature determination

In the study of the earth's surface dynamics, LST is a significant issue. The Mono-Window Algorithm (MWA) has been used in this paper to extract LST from Landsat satellite data (Guha and Govil 2017). This algorithm offers a straightforward and efficient approach for acquiring LST, which makes it easier to investigate and analyze the impacts of UHI (Y. Lu et al. 2009). The surface tem-

Table 1
LULC indices.

| Indices | Reference |
|--|-------------------------|
| NDVI = $\frac{NIR - RED}{NIR + RED}$ | (Tucker 1979) |
| NDBal = $\frac{SWIR - TIR}{SWIR + TIR}$ | (Zhao and Chen 2005) |
| NDBI = $\frac{SWIR - NIR}{SWIR + NIR}$ | (Zha, Gao, and Ni 2003) |

Table 2
Values of K1 and K2.

| | K1 | K2 |
|------|----------|-----------|
| LS-5 | 607.76 | 1260.56 |
| LS-7 | 666.09 | 1282.71 |
| LS-8 | 774.8853 | 1321.0789 |
| LS-9 | 799.0284 | 1329.2405 |

perature is calculated using Landsat imagery's thermal bands. Band 6 (10.40 m–12.50 m) is the thermal band for Landsat 5, and Landsat 7. And it's band 10 (10.6 μm–11.19 μm) for Landsat 8 and Landsat 9. These bands were applied to determine the temperature of the ground surface.

Initially, Eq. (1) was used to transform Digital Numbers (DNs) to radiance for Landsat 5, Landsat 7, and Eq. (2) for Landsat 8, and Landsat 9.

$$L_{\lambda} = \left(\frac{L_{\max\lambda} - L_{\min\lambda}}{QCal_{\max} - QCal_{\min}} \right) * (QCal - QCal_{\min}) + L_{\min\lambda} \quad (1)$$

Where, L_{λ} = sensor radiance, $L_{\max\lambda}$ = maximum radiance of band 6, $L_{\min\lambda}$ = minimum radiance of band 6,

$QCal$ = quantized calibrated pixel value in DN, $QCal_{\max}$ = max quantized calibrated pixel value in DN, and $QCal_{\min}$ = min quantized calibrated pixel value in DN.

$$L_{\lambda} = M_L * QCal + A_L \quad (2)$$

Where, M_L = radiance multiplicative scaling factor, A_L = radiance additive scaling factor for band 10, $QCal$ = pixel value in DN.

Eq (3) is applied to adjust for local sun elevation angles for band 1 to band 9, and LST is estimated using band 10 (10.6 μm–11.19 μm) of the Landsat 8 thermal data

$$L'_{\lambda} = \frac{L_{\lambda}}{\sin \theta_S} \quad (3)$$

θ_S is scene-center solar elevation angle in degrees,

Following the DN transformation, Eq. (4) is used to get the Brightness temperature (BT) in °C.

$$BT = \left(\frac{K_2}{\ln(\frac{K_1}{L'} + 1)} \right) - 273.15 \quad (4)$$

Where, K_1 & K_2 are the calibration constants of thermal bands, as shown in Table 2.

Then, the LST is determined using Eq. (5):

$$LST = \frac{BT}{1 + \left(\frac{\lambda \cdot BT}{\rho} \right)} * \ln(\varepsilon) \quad (5)$$

Where λ = is the central band wavelength of emitted radiance, BT = Brightness temperature,

and ε = emissivity (evaluated by using Eq. (6)):

$$\varepsilon = 0.004 * Pv + 0.986 \quad (6)$$

Where Pv = proportion of vegetation evaluated by using Eq. (7):

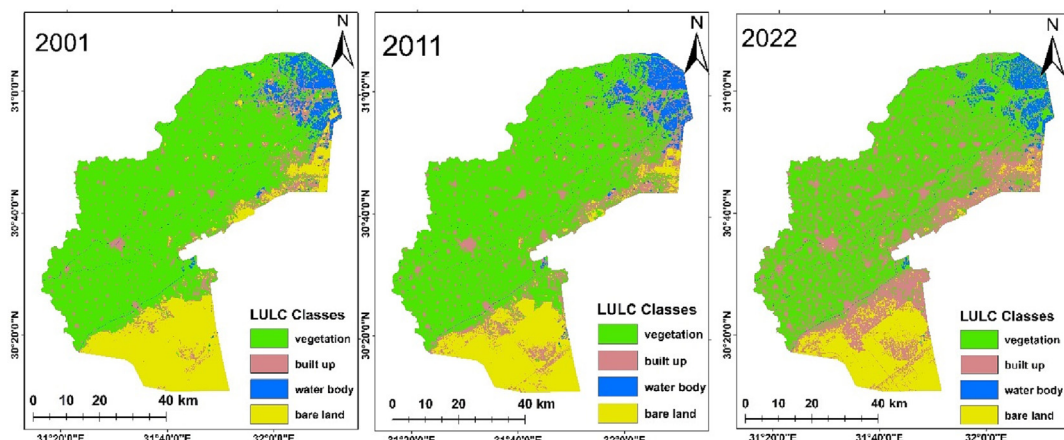


Fig. 3. LULC categories maps of Sharqiyah 2001, 2011, and 2022.

$$P\nu = \left(\frac{(NDVI - NDVI_{min})}{(NDVI_{max} - NDVI_{min})} \right)^2 \quad (7)$$

Where NDVI was already estimated. The map of LST distribution over Sharqiyah was created by classifying temperatures into suitable ranges and assigning them colors.

2.6. Mapping UHI, Non-UHI

The following equations were used to determine UHI and non-UHI regions (Guha et al. 2018):

$$LST > \mu + 0.5 * \sigma \quad (8)$$

$$0 < LST \leq \mu + 0.5 * \sigma \quad (9)$$

Where μ is the mean LST and σ is the standard deviation (STD) of LST in Sharqiyah, respectively. Using (Eq. (8)) UHI zones were derived as the areas with LST higher than the sum of the mean LST and 1/2 of STD. These areas are the hottest in the governorate. (Eq. (9)) reveals that the remainder of the governorate is Non-UHI.

3. Results and discussion

3.1. Land use land cover classification

For this research, SVM was utilized to classify the LULC. The LULC of Sharqiyah is divided into four classes (vegetation, built-up, bare land, and water bodies) based on Landsat pictures for

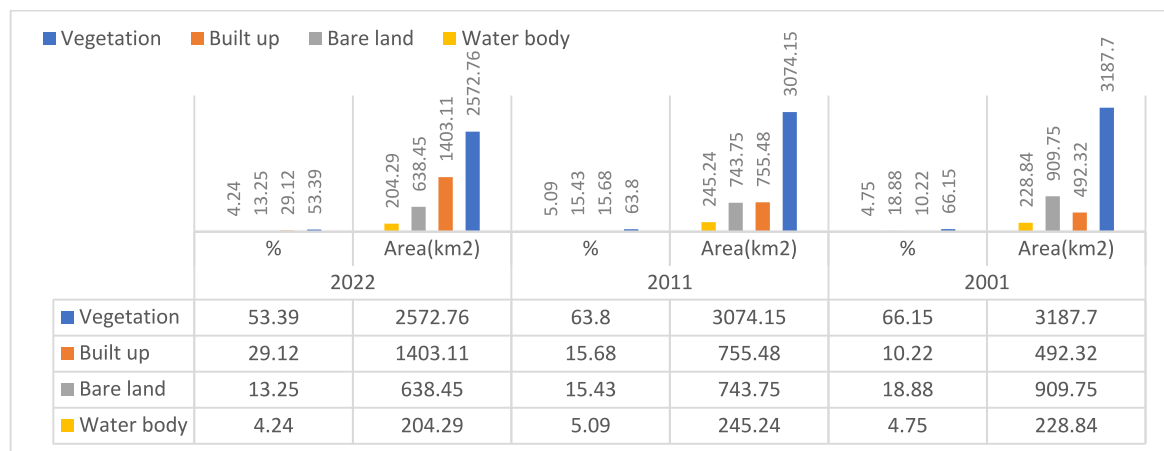


Fig. 4. Area and percentage of LULC classes distribution in 2001, 2011, and 2022.

Table 3

Map accuracy assessment for classified maps.

| | User Accuracy | | | | Producer Accuracy | | | | Overall-Accuracy | Kappa-coefficient |
|------|---------------|------------|--------------|-----------|-------------------|------------|--------------|-----------|------------------|-------------------|
| | Built-up | Vegetation | Water-bodies | Bare-Land | Built-up | Vegetation | Water-bodies | Bare-Land | | |
| 2001 | 90.63 | 94.58 | 85.71 | 93.41 | 91.58 | 93.45 | 83.33 | 95.51 | 92.53 | 0.89 |
| 2011 | 90.91 | 93.29 | 85.96 | 94.74 | 93.75 | 92.05 | 94.23 | 89.11 | 92 | 0.89 |
| 2022 | 92.73 | 93.53 | 90.57 | 92.59 | 92.73 | 94.89 | 88.89 | 91.46 | 92.69 | 0.90 |

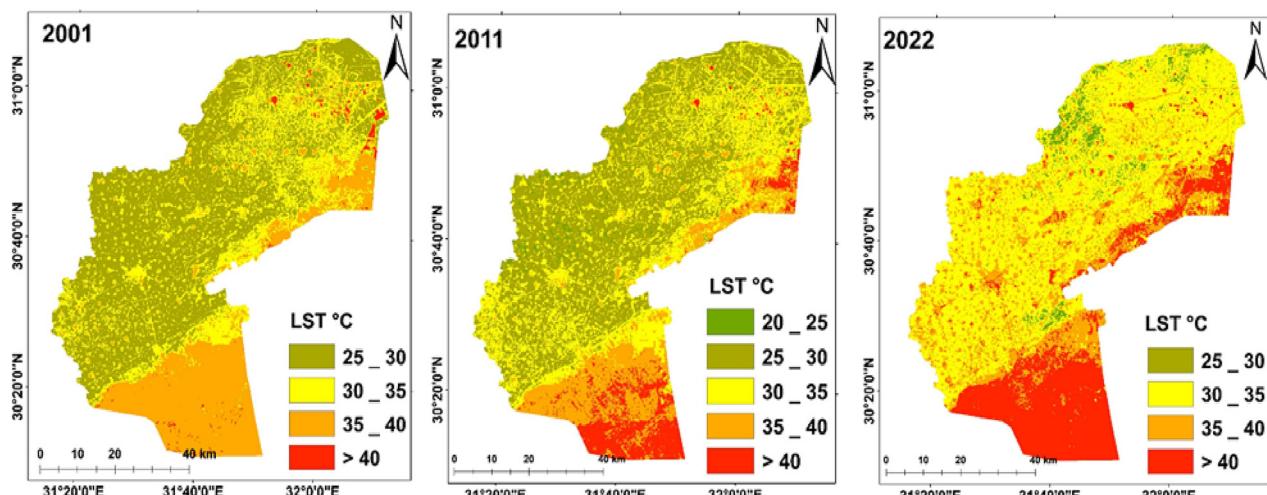


Fig. 5. Spatial variation of LST (°C) in Sharqiyah for 2001, 2011, and 2022.

three time periods (2001, 2011, and 2022). In 2001, vegetation covered the majority of the governorate area (66.15 %), with bare land accounting for 18.88 %. The results indicated fast changes in built-up areas and vegetation, as shown in Fig. 3. The percentage of built-up area is rising over time, covering a total area of 492.32 km² (10.22 %) in 2001, 755.48 km² (15.68 %) in 2011, and 1403.11 km² (29.12 %) in 2022, as shown in Fig. 4. In 2001, the percentage of vegetation cover accounted for about 66.15 %, decreased to 63.80 % by 2011, and was recorded at 53.39 % in 2022. Another type of land cover that has decreased over time is bare land. In 2001, the bare land covered about 18.88 %, 15.43 % in 2011, and decreased to 13.25 % by the year 2022. For the water body class, it decreased from 228.84 km² (4.75 %) in 2001 to 204.29 km² (4.24 %) in 2022. During the time of the study, the trend shows

an increase in the built-up area; furthermore, there is a decline in the vegetation cover. Uncontrolled urbanization due to increasing population, migration to cities, and infrastructure investment depletes natural resources like agricultural areas (Fu and Weng 2018).

Based on the error matrix used to evaluate the LU/LC maps' quality, the overall accuracy for the years 2001, 2011, and 2022 were 92.53 %, 92 %, and 92.69 %, respectively (Table 3). The user accuracy for all classes ranged from 85 % to 95 %. On the other hand, the producer's accuracy ranged from 83 % to 96 %. These results indicate trusted land cover categorization and good consistency between the referred and categorized maps (Dutta et al. 2021). Kappa coefficients were observed at 0.89, 0.89, and 0.90 in 2001, 2011, and 2022, respectively.

Table 4
LST zones in Sharqiyah for 2001, 2011, and 2022.

| | 2001 Area(km ²) | % | 2011 Area(km ²) | % | 2022 Area(km ²) | % |
|---------|--------------------------------|-------|--------------------------------|-------|--------------------------------|-------|
| 20 – 25 | 0.00 | 0.00 | 46.06 | 0.96 | 0.00 | 0.00 |
| 25 – 30 | 2418.49 | 50.19 | 2149.72 | 44.61 | 183.32 | 3.80 |
| 30 – 35 | 1247.00 | 25.88 | 1485.03 | 30.82 | 2588.79 | 53.72 |
| 35 – 40 | 1115.55 | 23.15 | 763.40 | 15.84 | 1054.30 | 21.88 |
| >40 | 37.56 | 0.78 | 374.41 | 7.77 | 992.20 | 20.59 |

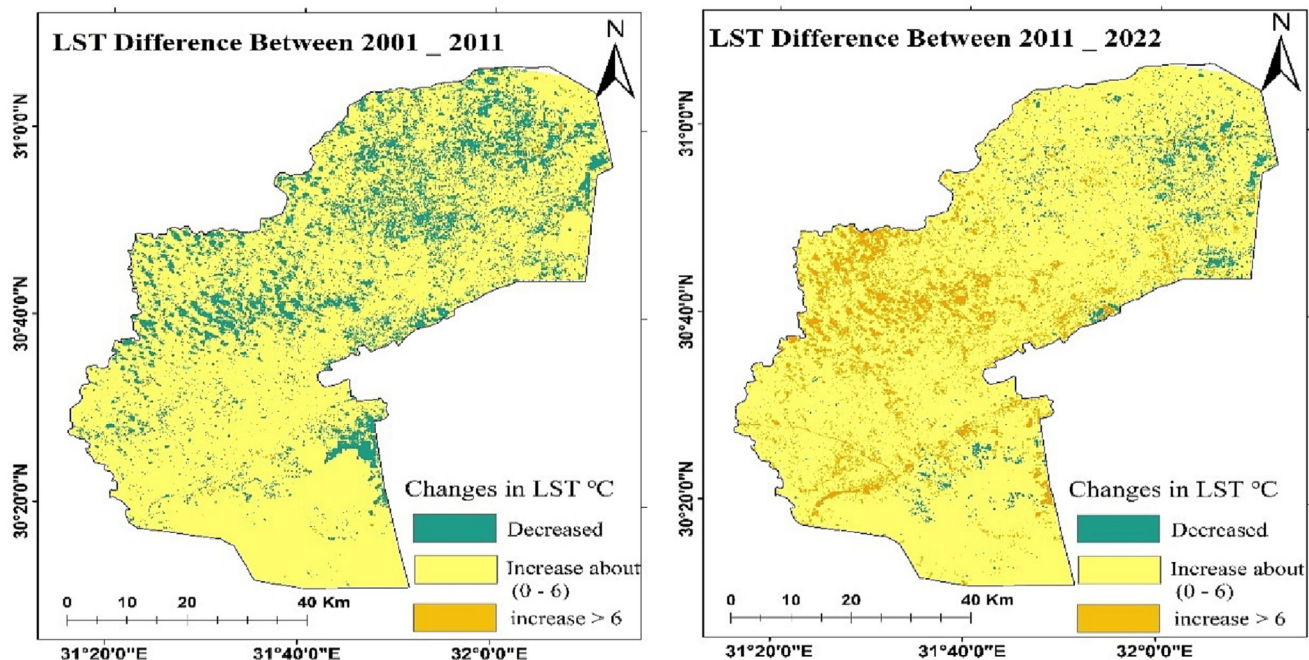


Fig. 6. Changes in LST between 2001 and 2011 and 2011–2022.

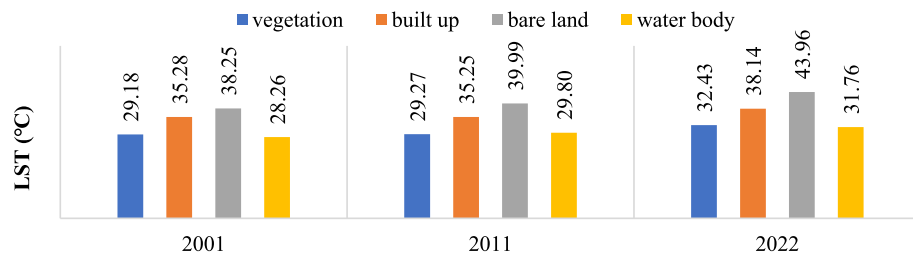


Fig. 7. Mean LST for vegetation, built-up, bare-land, and water-bodies classes.

3.2. Land surface temperature

Landsat thermal bands were used to figure out how the LST changed in different places during the summers of 2001, 2011, and 2022. As shown in Fig. 5, the shades of green to red represent lower to higher temperatures in the Sharqiyah Governorate for all years. Higher temperatures were noted in the governorate's southern parts in 2001, which were extended from 2001 to 2022. As

shown in Fig. 5, by 2022, there were large patches of reddish areas all over the governorate. This meant that the LST was changing quickly.

According to Table 4, the LST values were classified into five different temperature zones during the summer seasons of 2001, 2011, and 2022. From 2001 to 2022, the number of regions with surface temperatures ($>40^{\circ}\text{C}$) increased by 19.81 %, whereas the number of areas with surface temperatures (25–30 °C) decreased

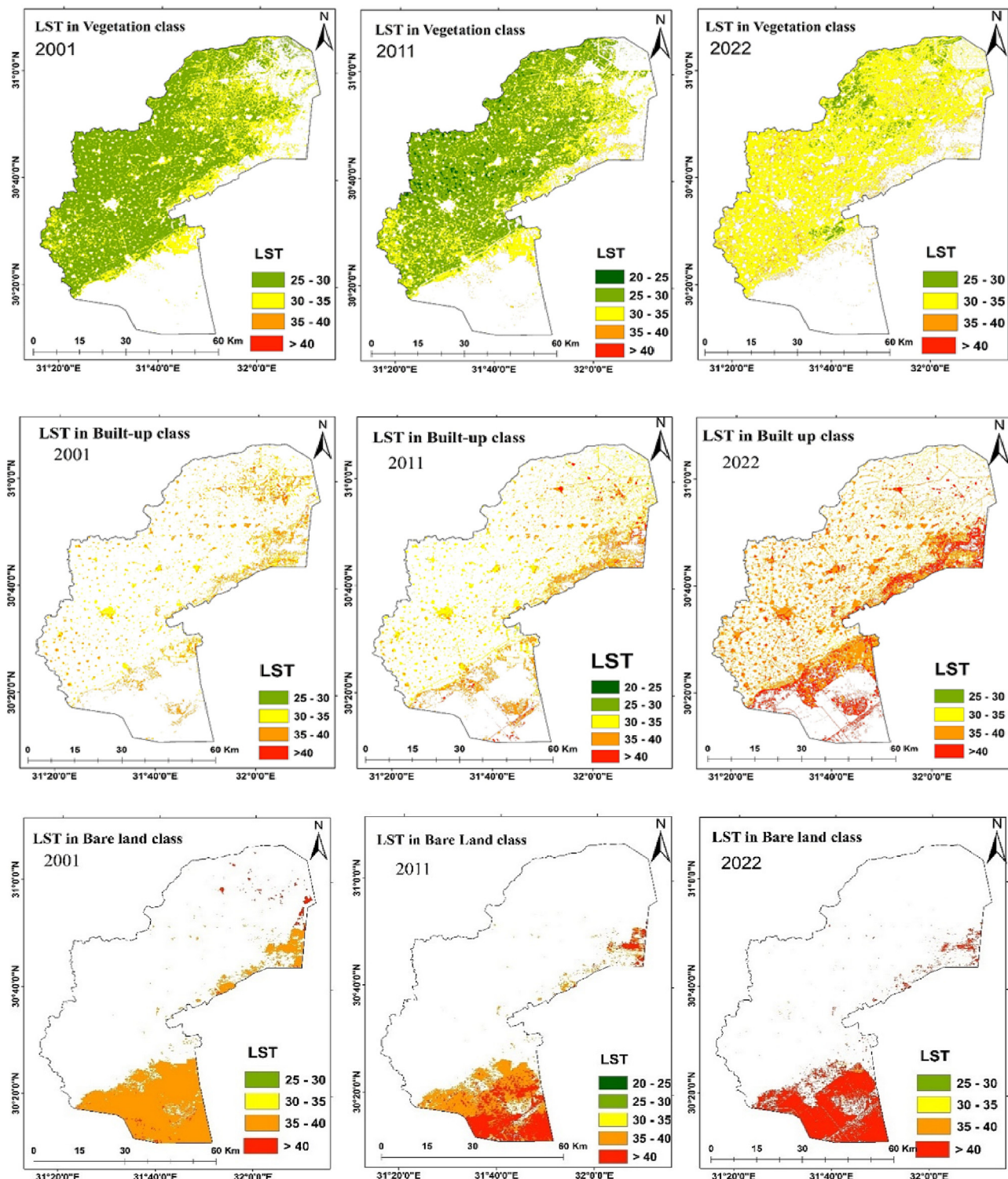


Fig. 8. LST distribution for each class in 2001, 2011, and 2022.

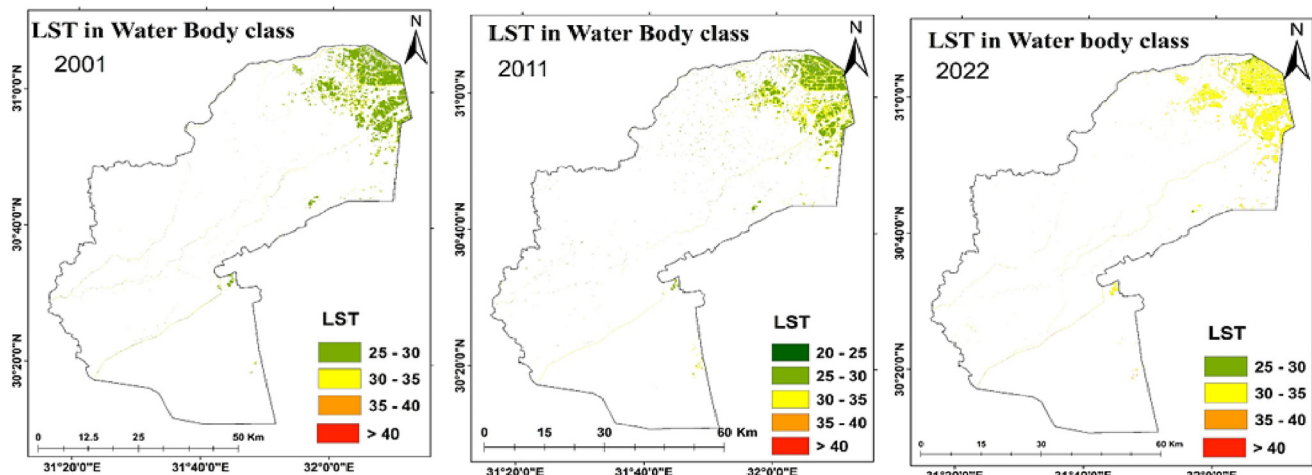


Fig. 8 (continued)

by -46.39% . The analysis shows that most of Sharqiyah were covered by four temperature zones in the summer of 2001: (25–30 °C), (30–35 °C), (35–40 °C), and (>40 °C). During the summer of 2001, a minor share of land was located in the temperature zone (>40 °C), although 7.77 % and 20.59 % of the land were noticed in the temperature zone (>40 °C) in 2011 and 2022, respectively. In 2011, 44.61 %, 30.82 %, and 15.84 % of the area were noted in the zones of (25–30 °C), (30–35 °C), and (35–40 °C), respectively, whereas in 2022, 3.80 % (183.32 km²), 53.72 % (2588.79 km²), and 21.88 % (1054.30 km²) were noted. According to the visible results, a smaller temperature zone was observed in Sharqiyah in 2001 and was turned into a higher temperature zone between 2011 and 2022.

From 2001 to 2011, there was an increase in LST in most of the regions of the governorate, especially in the southern part, as illustrated in Fig. 6. In other parts of the governorate, LST decreased, as indicated by green patches. From 2011 to 2022, there was a significant increase in LST across almost the entire region, with a notable increase of over 6 °C in the central part of the governorate, as shown by the orange patches in Fig. 6. However, in some small areas of the governorate, LST decreased. The findings suggest that the expansion of built-up areas and a decline in vegetation could potentially contribute to a large rise in temperatures, particularly during the interval from 2011 to 2022, when some regions experienced a temperature rise of >6 °C. These results highlight the critical role of LULC changes in affecting UHI and its associated impacts on LST changes. As a consequence, it is essential to include these outcomes in urban planning and management policies to reduce the negative effects of urbanization on the local climate and enhance the livability of urban areas.

3.3. Land surface temperature over different land uses and land covers

As Sharqiyah Governorate is largely covered by vegetation due to its status as an agricultural governorate, the vegetation and water body areas on the map have the least LST, as shown in Fig. 7 and Fig. 8. The thermal values of every land cover class were obtained by merging the LST image with a LULC map from the same time period to understand the link between urban development and LST. Fig. 7 shows the LST mean values for several land cover classes for each of the multi-temporal pictures. The bare lands have the greatest temperature, followed by the built-up regions.

The statistics of the LST of 2001 show that the mean temperature for the built-up areas in Sharqiyah was 35.28°C. From Fig. 7, and Fig. 8 it is clear that all bare land and built-up areas have sig-

nificantly high temperatures. This finding aligns with the outcomes that were obtained by (Effat and Hassan 2014). In bare land areas, the mean temperature was 38.25 °C, 2.97 °C higher than in urban areas. Despite the fact that temperature hotspots appeared in built-up regions. For 2011, according to the LST collected, built-up regions recorded a mean temperature of 35.25 °C. The mean temperature in the bare land regions was 39.99°C, 4.74 °C higher than in urban areas. In 2022, image measurements showed that the mean temperature in the built-up regions in Sharqiyah was 38.14°C. At the same time, the mean temperature in the bare land areas was 43.96°C, 5.82°C higher than the mean in urban areas. Noting the results, the mean LST for vegetation class increased by 3.25°C and water body class increased by 3.5°C from the year 2001 to 2022. And for the built-up class, LST rose by 2.86°C in the research period. Bare Land LST increased by 5.71°C throughout the study period. The bare land class had the largest increase in temperature.

LST of the vegetation class increased from 2001 to 2011 and showed a significant increase by 2022, predominantly falling within the temperature range of 30–35 °C, with some small patches observed in the range of 35–40 °C as shown in Fig. 8. Similarly, the LST of bare land and built-up areas significantly increased by 2022, with the majority of the bare land exhibiting temperatures >40 °C. In built-up areas, the temperature range of >40 °C became Existing, while the range of 35–40 °C became more widespread.

3.4. Spatiotemporal distribution of LULC indices

The LULC index maps of Sharqiyah are represented in Fig. 9 for the years 2001, 2011, and 2022. The NDBal maps were used to represent the spatial variation of bareness concentration. As shown in Fig. 9, the governorate's southern parts had the maximum distributed NDBal at all study times because of the occurrence of a heavy bare land region as desert areas (10th of Ramadan city), while the rest of the governorate had minimum NDBal. The NDBI maps were used to represent the spatial variation of building concentration. The largest distributed NDBI was detected in several regions in the governorate's center as a result of densely built-up regions and bare land, while the weakest NDBI was found in the rest of the governorate due to the presence of vegetation. Maps of NDVI represent the spatial changes in vegetation distribution. The lowest-distributed NDVI was detected in southern parts and in some batches in the governorate's center because of the occur-

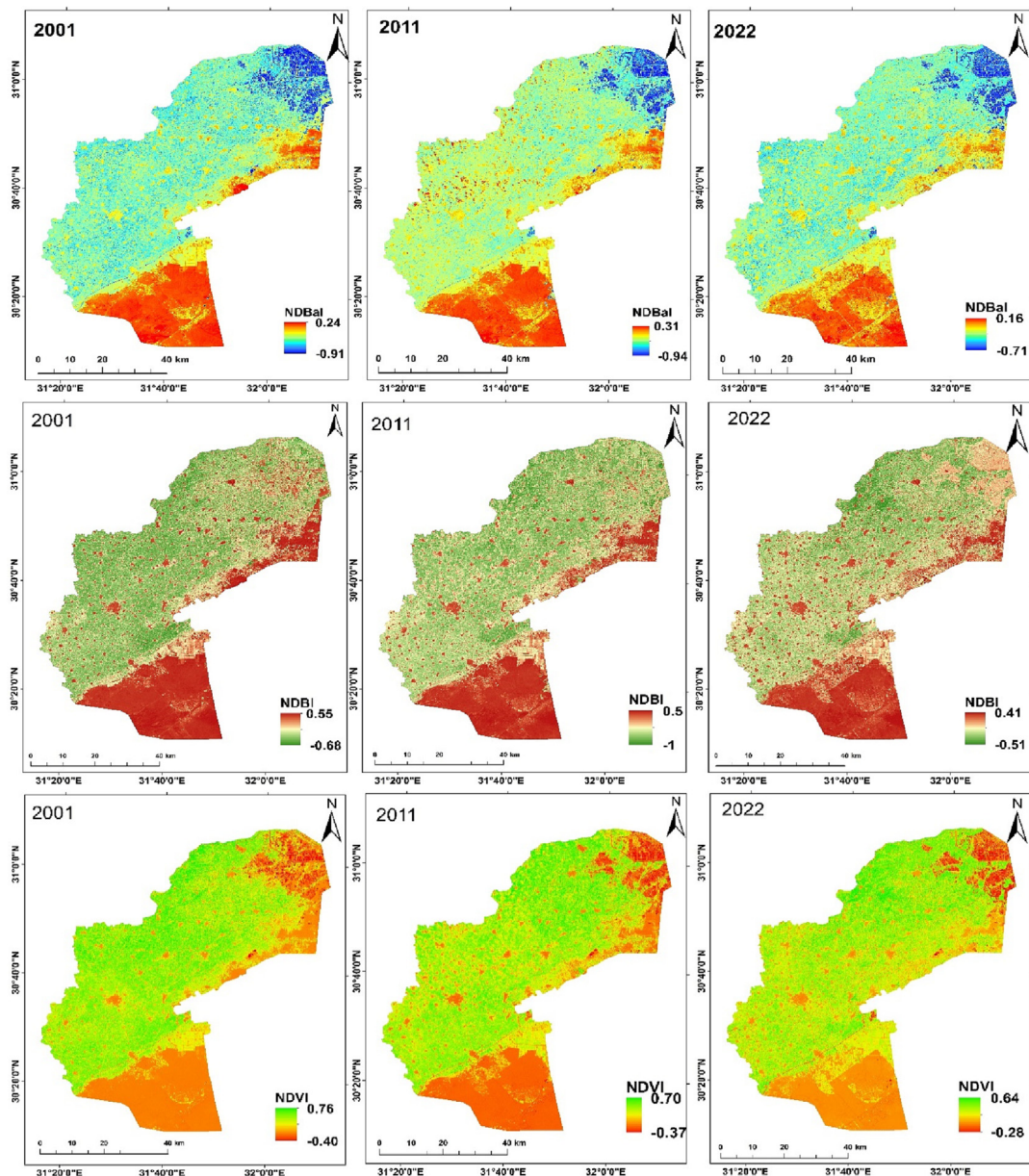


Fig. 9. LULC indices for 2001, 2011, and 2022.

rence of bare land and built-up areas. NDVI maps showed a decrease in NDVI density during the study period.

3.5. Relationship between LST and LULC indices

Global population growth is one of the reasons for increasing stress on natural environmental supplies and extreme growth in LST, which has a direct impact on LULC properties (Feizizadeh and Blaschke 2013). LST increases have an effect on the formation of UHIs (A. Al Kafy et al., 2021b). Studying LULC changes is essential for determining regional climate changes. However, for the calculation of LST, LULC data are needed. LST has a statistical correlation with these three indices. The NDBI and NDBal have a positive correlation with the LST, this result aligns with the observations of (Mansour et al. 2022), as the heat emitted from buildings contributes to an increase in LST (Kaplan et al., 2018). The NDVI value is inversely proportional, as shown in Fig. 10. Similar to (Guha et al. 2018). This is acceptable because NDVI values varied

from dense to poor vegetation and, in some cases, bare land. In spatiotemporal analysis, densely vegetated areas generate greater NDVI values. As a result, the denser the vegetation, the lower the LST. Each correlation test's p-value has been less than 0.05, indicating that the testing processes were statistically acceptable. The R^2 values indicated a good relationship in the analysis of LST with NDVI, NDBI, and NDBal for each of the three study periods (2001, 2011, and 2022).

3.6. Urban Heat Island distribution

The study's results found that UHI spatial distribution followed virtually the same pattern during the study period. Throughout the study period, Sharqiyah's south part has the highest density of UHI areas, as shown Fig. 11. Whereas the temporal pattern of UHI areas has remained consistent across the study period, as shown in Table 5, their intensity has grown in the center because of the growth of built-up regions and decreasing vegetation. Additionally,

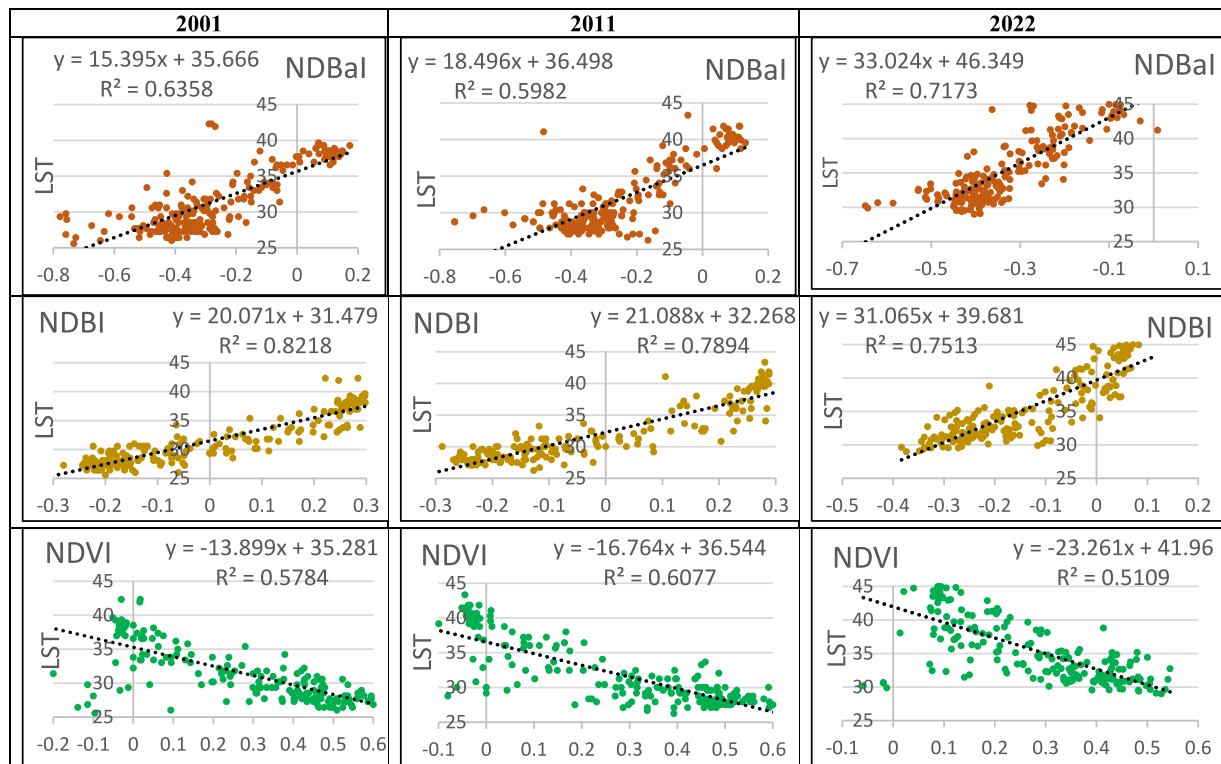


Fig. 10. Linear correlation plot between LST and LULC indices.

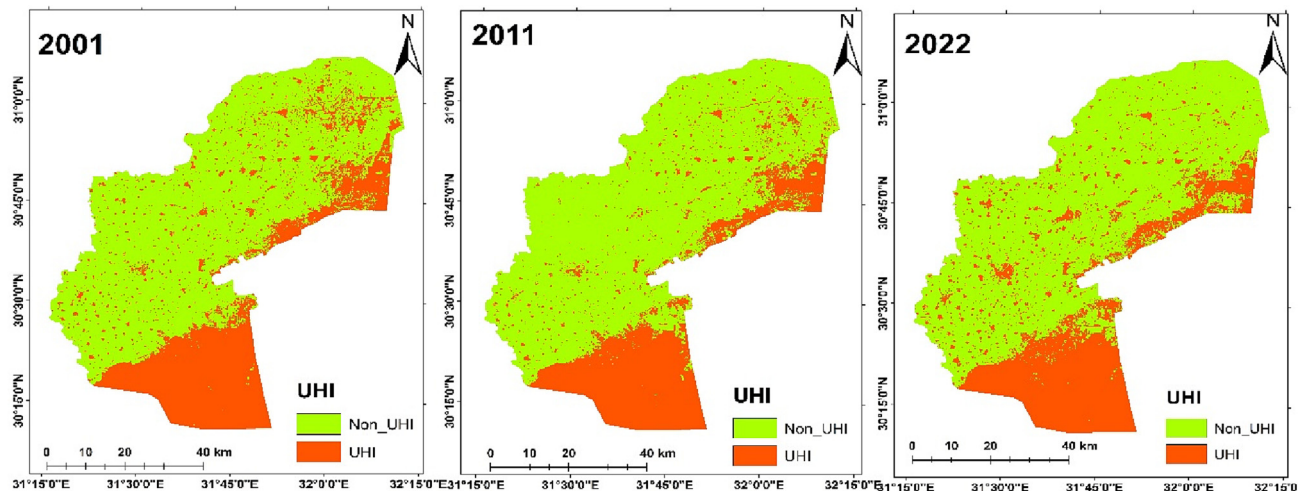


Fig. 11. Spatiotemporal distribution for uhi and non-uhi areas in Sharqiyah 2001, 2011, and 2022.

Table 5

Temporal distribution area for UHI and Non-UHI in 2001, 2011, and 2022.

| | 2001 | 2011 | 2022 | |
|---------|------------------------|-------|------------------------|-------|
| | Area(km ²) | % | Area(km ²) | % |
| Non-UHI | 3428.69 | 71.16 | 3566.09 | 74.01 |
| UHI | 1389.91 | 28.84 | 1252.52 | 25.99 |

the UHI is caused by the bare land, which is in the form of a desert (**Abulibdeh 2021**). The UHI threshold temperature in Sharqiyah increased significantly between 2001 and 2022 by 4.27°C, as shown in details in **Table 6**, despite some variance in its distribution.

Table 7 displays the LST values for UHI and non-UHI zones. The mean LST values grew substantially from 2001 to 2022. The maximum LST values in UHI areas showed a higher increase of 6°C during the study period. In Non-UHI zones, maximum LST values

increased by 4.39°C the minimum and mean LST values increased by a smaller amount. In 2001, the maximum LST for UHI was 42.31°C and increased to 43.34°C in 2011, and in 2022, there was a large increase to 48.31°C. Min LST in 2001 for the UHI zone was 33.81°C, then grew to 34.76°C in 2011, and in 2022, min LST reached 38.15°C. For mean LST, it was 37.37°C in 2001, then increased to 38.86°C in 2011, and in 2022 it grew to 42.37°C. According to LST values in Table 7, it was noticed that the max, min, and mean LST in UHI areas are larger than LST values in Non-UHI. The mean LST in 2001 was 29.09°C, 29.39°C in 2011, and in 2022 it reached 32.93°C in Non-UHI areas. Max LST values in Non-UHI reached 37.80°C in 2022, although they were 34.06°C in 2011 and 33.41°C in 2001.

3.7. Analysis of the variation in LST using data from the Landsat satellite and MODIS

The average of the temperature measurements calculated from the scene photos was chosen as the summer LST of Sharqiyah.

Table 6
Mean LST and UHI threshold temperature.

| LST(°C) | 2001 | 2011 | 2022 |
|--------------------|-------|-------|-------|
| μ | 31.47 | 32.39 | 35.45 |
| σ | 4.14 | 4.53 | 4.71 |
| $\mu+0.5 * \sigma$ | 33.54 | 34.66 | 37.81 |

Table 7
Statistics of UHI and Non-UHI LST for 2001, 2011, and 2022.

| | UHI(°C) | | | Non-UHI(°C) | | |
|------|---------|-------|-------|-------------|-------|-------|
| | Max | Min | Mean | Max | Min | Mean |
| 2001 | 42.31 | 33.81 | 37.37 | 33.41 | 25.59 | 29.09 |
| 2011 | 43.34 | 34.76 | 38.86 | 34.06 | 24.12 | 29.39 |
| 2022 | 48.31 | 38.15 | 42.37 | 37.80 | 28.75 | 32.93 |

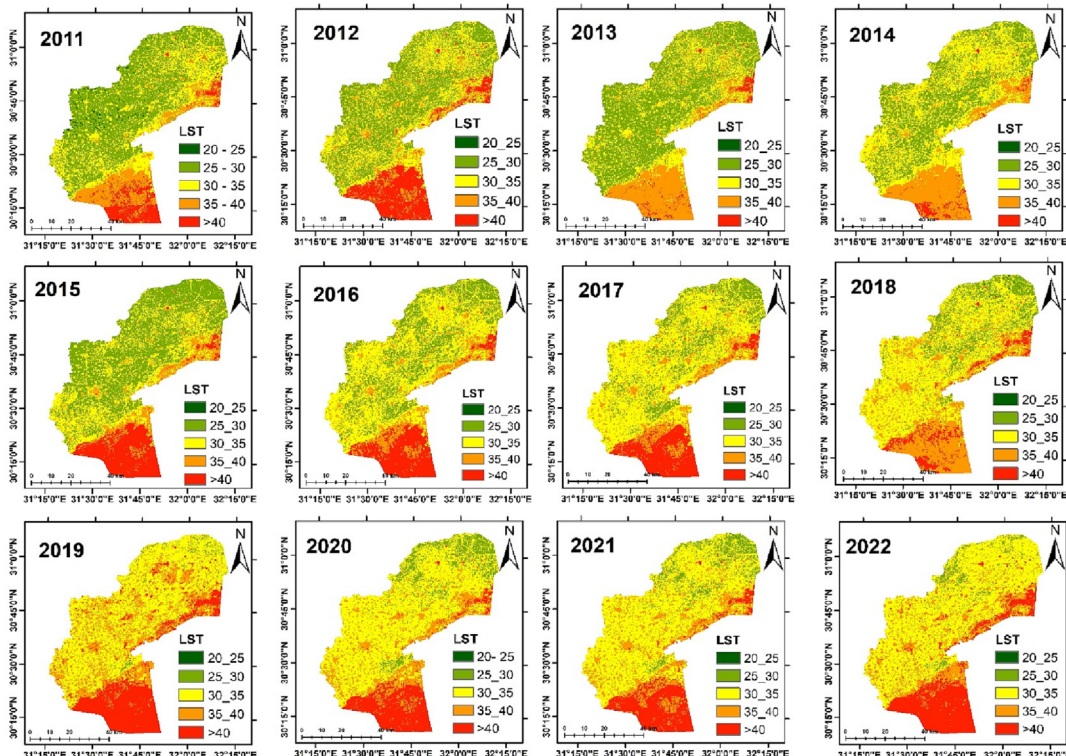


Fig. 12. Land surface temperature maps from 2011 to 2022.

Fig. 12 shows that high-temperature results were focused in urban towns and bare land areas. The outputs of the Landsat LST collection, given in Table 8, indicate a comparable fluctuation in temperature during the summer. As a result, it was challenging to determine an average climatic value that was constant across the research area. It is challenging to evaluate the increase in temperatures associated with the expansion of urban areas based only on Landsat results. Thus, the MODIS satellite and air temperature measurements derived from the NWP technique were used to compare temperatures. The findings for increasing temperatures are acceptable, and this pattern was detected after comparing various datasets. Despite the considerable variance between the two sensors, it is certain that the measured temperature is true due to the growing temperature trend.

3.8. Verification of LST

The LST data must be validated to confirm the validity of the outcomes. We collected data produced from MODIS images. Some difficulties with this form of validation deal with unreliability in accuracy, including the correct measurement of the imagery. To resolve these issues, the NWP for air temperature measurements was utilized. NWP (ERA5, the most recent edition of the Copernicus Climate Change Service's atmospheric reanalysis of global climate) obtained the air temperature values. As a result, the datasets Landsat and MODIS can be used as valid guidelines for the air temper-

Table 8

Temperature in °C using Landsat, MODIS, and NWP.

| | Landsat Max | Min | Mean | Temperature(°C) | | | NWP Max | Min | Mean |
|---------|----------------|-------|-------|-----------------|-------|-------|------------|-------|-------|
| | | | | MODIS Max | Min | Mean | | | |
| Jul2011 | 43.34 | 26.25 | 32.39 | 48.17 | 31.69 | 37.63 | 39.62 | 23.32 | 31.87 |
| Aug2012 | 45.71 | 27.35 | 32.88 | 45.07 | 30.63 | 35.68 | 38.43 | 25.75 | 31.69 |
| Jul2013 | 44.42 | 26.37 | 32.07 | 49.99 | 31.97 | 37.54 | 38.75 | 25.55 | 31.81 |
| Aug2014 | 41.74 | 27.49 | 32.75 | 48.17 | 31.53 | 36.95 | 38.23 | 25.70 | 31.52 |
| Aug2015 | 43.91 | 26.40 | 32.47 | 47.31 | 31.33 | 37.16 | 41.34 | 26.06 | 32.81 |
| Jul2016 | 44.09 | 27.93 | 33.44 | 49.55 | 32.03 | 37.64 | 39.54 | 25.06 | 32.26 |
| Jul2017 | 44.28 | 27.70 | 33.83 | 48.31 | 32.45 | 37.10 | 42.19 | 25.47 | 34.29 |
| Aug2018 | 44.36 | 27.73 | 34.00 | 46.87 | 30.85 | 36.33 | 37.73 | 25.78 | 30.89 |
| Aug2019 | 41.80 | 22.51 | 32.70 | 47.73 | 31.09 | 36.48 | 38.38 | 26.38 | 31.46 |
| Jul2020 | 43.52 | 28.54 | 34.49 | 48.39 | 31.17 | 37.42 | 40.52 | 23.69 | 32.84 |
| Jul2021 | 43.34 | 24.53 | 34.62 | 48.99 | 32.09 | 38.21 | 41.70 | 24.66 | 33.73 |
| Jul2022 | 45.71 | 28.53 | 35.45 | 48.19 | 31.53 | 36.92 | 40.44 | 25.50 | 32.84 |

Table 9

RMSE of LST values.

| | Landsat/MODIS Max | Min | Mean | MODIS/NWP Max | Min | Mean | Landsat/NWP Max | Min | Mean |
|------|----------------------|------|------|------------------|------|------|--------------------|------|------|
| RMSE | 4.63 | 5.07 | 3.84 | 8.47 | 6.39 | 4.83 | 4.45 | 2.58 | 1.49 |

ture observed by the NWP technique. **Table 8** gives the maximum and minimum values every month according to the Landsat and Modis collection time frames. According to NWP records in **Table 8**, the maximum observed temperature was 42.19°C, and the least observed temperature was 23.32°C. After averaging the LST values collected for the years 2011 to 2022, the corresponding Root Mean Square Error (RMSE) values were calculated as in **Table 9**. Due to its reliability and accuracy, Landsat was used as the standard LST for air temperature. It is clear that, when compared, both LST and NWP measurements have the smallest value among the various datasets. Regarding the nature of the sample, the results are respectable and stable, with an RMSE of 4.45 and 2.58 °C for the highest and lowest readings, respectively. Based on seasonal variation, (Kenawy et al., 2019) estimated that the average RMSE temperature in Egypt was 5 °C. Research in other parts of the world has indicated that MODIS may be used to determine air temperature. (L. Lu et al. 2018) reported an RMSE ranging from 2.39 to 3.05°C, depending on seasonal and climate variance. (Zhu, Lü, and Jia 2013) also used MODIS as well as air temperature on the North Tibetan Plateau of China to calculate an RMSE of 7.45°C and a bias of 6.21°C. This higher result was a result of cloudy pixels and mist enclosing the study region, which was the reason for them. These findings are in line with the results of the current research, from which we deduced RMSE values ranging from 4.45 to 2.58°C for various sensor comparisons. The RMSE should be between 4 and 5°C if the investigation were carried out in the summer.

4. Conclusion

The LST is an essential issue in the climate mechanism on Earth. Landsat-5, Landsat-7, Landsat-8, and Landsat-9 images were collected from the USGS. Using data from Landsat, this research evaluates the LULC and LST during the study period. Urban development and climate variation both lead to a rise in land surface temperature. When we compare vegetation and built-up regions, the built-up area has higher LST values. Landsat imagery data analysis has been researched to estimate the extent of the UHI-impacted region from 2001 to 2022 and the impact of LULC variations on the LST. The LST grew quickly, especially in urban

areas and desert/bare land. The utilization of Landsat with the MWA technique produced acceptable results; however, outliers occurred as an outcome of the preprocessing step. Over the study period, the built-up regions rose considerably (10.22 % to 29.12 %). In contrast, vegetation reduced substantially from 66.15 % to 53.39 %, and bare land decreased by 5.63 %. Variations in LULC have also impacted the allocation of land cover regions over time, especially the transition of land cover classes from previously vegetated land to urban zones or towards more bare land. As a result, the distribution of UHI areas has increased over time, while mean LST has risen rapidly with decreasing waterbodies and vegetation. The major goal of this research was to identify variations in LULC and land surface temperature caused by development in Sharqiyah. It was also shown that vegetation and LST have a negative correlation. In contrast, built-up regions and bare land have a positive correlation with LST. The study's findings give a complete knowledge of the causes of growing LST, which are mostly related to increased urbanization and, as a result, the spread of agricultural land encroachment. However, preventing urbanization without a shift in high-level management decisions is difficult. There were several challenges observed when doing the research. For instance, satellite images were collected at different times. If these images had been acquired at the same time, the results would have been more dependable and accurate. An important limitation of this study is that results may be affected when there are partially cloudy conditions, as clouds can cause abnormal values in the data. If the satellite data's geospatial accuracy had been higher, the LC classification would be more accurate. This research has significant implications for future environmental science research. To further investigate the impact of other environmental factors on LULC changes and LST, such as precipitation, humidity, and wind patterns, policymakers and urban planners can make more informed decisions to manage urban growth and minimize its negative impact on the environment and human health. Spectral indices such as Enhanced Vegetation Index (EVI), Soil Adjusted Vegetation Index (SAVI), and Normalized Difference Moisture Index (NDMI) can be estimated from surface reflectance data. Advanced remote sensing technologies, such as Sentinel data and radar, can be used to detect and monitor urban areas more accurately, particularly in rapidly urbanizing areas like Sharqiyah,

to identify trends and patterns over time with greater accuracy and inform policy decisions to mitigate UHI areas and the negative impacts of urbanization.

Declaration of Competing Interest

The authors declare that they have no known competing financial interests or personal relationships that could have appeared to influence the work reported in this paper.

References

- Abulibdeh, A., 2021. Analysis of Urban Heat Island Characteristics and Mitigation Strategies for Eight Arid and Semi-Arid Gulf Region Cities. *Environ. Earth Sci.* 80, 1–26.
- Bokaie, M., Zarkesh, M.K., Arasteh, P.D., Hosseini, A., 2016. Assessment of Urban Heat Island Based on the Relationship between Land Surface Temperature and Land Use/Land Cover in Tehran. *Sustain. Cities Soc.* 23, 94–104.
- Chen, X.L., Zhao, H.M., Li, P.X., Yin, Z.Y., 2006. Remote Sensing Image-Based Analysis of the Relationship between Urban Heat Island and Land Use/Cover Changes. *Remote Sens. Environ.* 104 (2), 133–146. <https://doi.org/10.1016/j.rse.2005.11.016>.
- Choe, Y.-J., Yom, J.-H., 2020. Improving Accuracy of Land Surface Temperature Prediction Model Based on Deep-Learning. *Spat. Inf. Res.* 28, 377–382.
- Dutta, Dipanwita, Atiqur Rahman, S. K. Paul, and Arnab Kundu. 2021. "Impervious Surface Growth and Its Inter-Relationship with Vegetation Cover and Land Surface Temperature in Peri-Urban Areas of Delhi." *Urban Climate* 37 (March): 100799. 10.1016/j.ulclim.2021.100799.
- Effat, H.A., Hassan, O.A.K., 2014. Change Detection of Urban Heat Islands and Some Related Parameters Using Multi-Temporal Landsat Images; a Case Study for Cairo City, Egypt. *Urban Clim.* 10, 171–188.
- Elbeih, S.F., El-Zeiny, A.M., 2018. Qualitative Assessment of Groundwater Quality Based on Land Use Spectral Retrieved Indices: Case Study Sohag Governorate, Egypt. *Remote Sens. Appl.: Soc. Environ.* 10 (April), 82–92. <https://doi.org/10.1016/j.rsase.2018.03.001>.
- El-Magd, I.A., Ismail, A., Zanaty, N., 2016. Spatial Variability of Urban Heat Islands in Cairo City, Egypt Using Time Series of Landsat Satellite Images. *Int. J. Adv. Rem. Sens. Syst.* 5 (1), 1618–1638. <https://doi.org/10.23953/cloud.ijarsg.48>.
- El-Zeiny, A.M., Effat, H.A., 2017. Environmental Monitoring of Spatiotemporal Change in Land Use/Land Cover and Its Impact on Land Surface Temperature in El-Fayoum Governorate, Egypt. *Remote Sens. Appl.: Soc. Environ.* 8 (November), 266–277. <https://doi.org/10.1016/j.rsase.2017.10.003>.
- Fadhil, Mohammed, Mustafa N Hamoodi, and Abdul Razzak T Ziboon. 2023. "Mitigating Urban Heat Island Effects in Urban Environments: Strategies and Tools." In *IOP Conference Series: Earth Environ. Sci.*, 1129:12025. IOP Publishing.
- Feizizadeh, B., Blaschke, T., 2013. Examining Urban Heat Island Relations to Land Use and Air Pollution: Multiple Endmember Spectral Mixture Analysis for Thermal Remote Sensing. *IEEE J. Sel. Top. Appl. Earth Obs. Remote Sens.* 6 (3), 1749–1756. <https://doi.org/10.1109/JSTARS.2013.2263425>.
- Fu, P., Weng, Q., 2018. Responses of Urban Heat Island in Atlanta to Different Land-Use Scenarios. *Theor. Appl. Climatol.* 133, 123–135.
- Guha, S., Govil, H., 2017. Dynamic Analysis and Ecological Evaluation of Urban Heat Islands in Raipur City, India. *J. Appl. Remote Sens.* 11 (August), 1. <https://doi.org/10.1117/1.JRS.11.036020>.
- Guha, S., Govil, H., Dey, A., Gill, N., 2018. Analytical Study of Land Surface Temperature with NDVI and NDBI Using Landsat 8 OLI and TIRS Data in Florence and Naples City, Italy. *Europ. J. Remot. Sens.* 51 (1), 667–678. <https://doi.org/10.1080/22797254.2018.1474494>.
- Hunt, J.C.R., Aktas, Y.D., Mahalov, A., Moustaqui, M., Salamanca, F., Georgescu, M., 2017. Climate Change and Growing Megacities: Hazards and Vulnerability. *Proceed. Institut. Civil Eng.: Eng. Sustainab.* 171 (6), 314–326. <https://doi.org/10.1680/jensu.16.00068>.
- Jimenez-Munoz, J.C., Cristobal, J., Sobrino, J.A., Sòria, G., Ninyerola, M., Pons, X., 2009. Revision of the Single-Channel Algorithm for Land Surface Temperature Retrieval from Landsat Thermal-Infrared Data. *IEEE Trans. Geosci. Remote Sens.* 47 (1), 339–349. <https://doi.org/10.1109/TGRS.2008.2007125>.
- Johnson, G.T., Oke, T.R., Lyons, T.J., Steyn, D.G., Watson, I.D., Voogt, J.A., 1991. Simulation of Surface Urban Heat Islands under 'IDEAL' Conditions at Night Part 1: Theory and Tests against Field Data. *Bound.-Lay. Meteorol.* 56 (3), 275–294.
- Jones, P.D., Wigley, T.M.L., Wright, P.B., 1986. Global Temperature Variations between 1861 and 1984. *Nature* 322 (6078), 430–444.
- Justice, C.O., Louis Giglio, S., Korontzi, J.O., Morisette, J.T., Roy, D., Descloitres, J., Alleaume, S., Petitcolin, F., Kaufman, Y., 2002. The MODIS Fire Products. *Remote Sens. Environ.* 83 (1–2), 244–262.
- Kafy, Abdulla Al, Abdullah Al Faisal, Md Shahinoor Rahman, Muhamminul Islam, Abdulla Al Rakib, Md Arshadul Islam, Md Hasib Hasan Khan, et al. 2021a. "Prediction of Seasonal Urban Thermal Field Variance Index Using Machine Learning Algorithms in Cumilla, Bangladesh." *Sustainable Cities and Society* 64 (October 2020): 102542. 10.1016/j.scs.2020.102542.
- Kafy, Abdulla Al, Abdullah Al Faisal, Md Shahinoor Rahman, Muhamminul Islam, Abdulla Al Rakib, Md Arshadul Islam, Md Hasib Hasan Khan, et al., 2021b. "Prediction of Seasonal Urban Thermal Field Variance Index Using Machine Learning Algorithms in Cumilla, Bangladesh." *Sustainable Cities and Society* 64 (January). 10.1016/j.scs.2020.102542.
- Kafy, A.-A., Foyezur Rahman, A.N.M., Rakib, A.A., Akter, K.S., Raikwar, V., Amir, D.M., Jahir, J.F., Kona, M.A., 2021. Assessment and Prediction of Seasonal Land Surface Temperature Change Using Multi-Temporal Landsat Images and Their Impacts on Agricultural Yields in Rajshahi, Bangladesh. *Environ. Challenges* 4, 100147.
- Kaplan, Gordana, Ugur Avdan, and Zehra Yigit Avdan. 2018. "Urban Heat Island Analysis Using the Landsat 8 Satellite Data: A Case Study in Skopje, Macedonia." In , 358. MDPI AG. 10.3390/ecrs-2-05171.
- Kenawy, Ahmed M. El, Mohamed E. Hereher, and Sayed M. Robaa. 2019. "An Assessment of the Accuracy of MODIS Land Surface Temperature over Egypt Using Ground-Based Measurements." *Remote Sensing* 11 (20). 10.3390/rs11202369.
- Lee, S., Hong, S.M., Jung, H.S., 2017. A Support Vector Machine for Landslide Susceptibility Mapping in Gangwon Province, Korea. *Sustainability (Switzerland)* 9 (1). <https://doi.org/10.3390/su9010048>.
- Liu, K., Hongbo, S.U., Li, X., Wang, W., Yang, L., Liang, H., 2016. Quantifying Spatial-Temporal Pattern of Urban Heat Island in Beijing: An Improved Assessment Using Land Surface Temperature (LST) Time Series Observations from LANDSAT, MODIS, and Chinese New Satellite GaoFen-1. *IEEE J. Sel. Top. Appl. Earth Obs. Remote Sens.* 9 (5), 2028–2042.
- Lo, C.P., Shipman, R.L., 1990. A GIS Approach to Land-Use Change Dynamics Detection. *Photogramm. Eng. Remote Sens.* 56 (11), 1483–1491.
- Lu, Y., Feng, X., Xiao, L., Shen, C., Sun, J., 2009. Urban Heat Island in Summer of Nanjing Based on TM Data. In: In 2009 Joint Urban Remote Sensing Event. IEEE, pp. 1–5.
- Lu, L., Zhang, T., Wang, T., Zhou, X., 2018. Evaluation of Collection-6 MODIS Land Surface Temperature Product Using Multi-Year Ground Measurements in an Arid Area of Northwest China. *Remote Sens. (Basel)* 10 (11), 1852.
- Mansour, K., Aziz, M.A., Hashim, S., Effat, H., 2022. Impact of Anthropogenic Activities on Urban Heat Islands in Major Cities of El-Minya Governorate, Egypt. *Egypt. J. Remote Sens. Space Sci.* 25 (2), 609–620.
- Mundhe, Nitin N, and Ravindra G Jaybhaye. 2014. "Impact of Urbanization on Land Use/Land Covers Change Using Geo-Spatial Techniques." *INT. J. GEOMAT. GEOSCI.* Vol. 5.
- Muñoz Sabater, J. 2019. "ERA5-Land Hourly Data from 1981 to Present, Copernicus Climate Change Service (C3S) Climate Data Store (CDS)[Data Set]."
- Ogashawara, I., Bastos, V., 2012. A Quantitative Approach for Analyzing the Relationship between Urban Heat Islands and Land Cover. *Remote Sens. (Basel)* 4 (11), 3596–3618. <https://doi.org/10.3390/rs4113596>.
- Owen, T.W., Carlson, T.N., Gillies, R.R., 1998. An Assessment of Satellite Remotely-Sensed Land Cover Parameters in Quantitatively Describing the Climatic Effect of Urbanization. *Int. J. Remote Sens.* 19 (9), 1663–1681.
- Pal, S., Ziaul, S.k., 2017. Detection of Land Use and Land Cover Change and Land Surface Temperature in English Bazar Urban Centre. *Egypt. J. Remote Sens. Space Sci.* 20 (1), 125–145. <https://doi.org/10.1016/j.ejrs.2016.11.003>.
- Qin, Z., Karniel, A., Berliner, P., 2001. A Mono-Window Algorithm for Retrieving Land Surface Temperature from Landsat TM Data and Its Application to the Israel-Egypt Border Region. *Int. J. Remote Sens.* 22 (18), 3719–3746. <https://doi.org/10.1080/01431160010006971>.
- Rakib, Abdulla Al, Shahed Mahmud Ayan, Tayaba Tabassum Orthy, Oma Sarker, Labib Intisar, and Masfiq Anzum Arnob. 2020. "In Depth-Analysis of Urban Resident-Satisfaction Level of Mirpur, Dhaka, Bangladesh: A Participatory Approach." *1st International Student Research Conference 2020*, no. December.
- Ramachandra, T.V., Bharath, S., Gupta, N., 2018. Modelling Landscape Dynamics with LST in Protected Areas of Western Ghats, Karnataka. *J. Environ. Manage.* 206, 1253–1262. <https://doi.org/10.1016/j.jenvman.2017.08.001>.
- Rimal, B., Zhang, L., Keshtkar, H., Wang, N., Lin, Y.i., 2017. Monitoring and Modeling of Spatiotemporal Urban Expansion and Land-Use/Land-Cover Change Using Integrated Markov Chain Cellular Automata Model. *ISPRS Int. J. Geo Inf.* 6 (9), 288.
- Rousta, Iman, Md Omar Sarif, Rajan Dev Gupta, Haraldur Olafsson, Manjula Ranagalage, Yuji Murayama, Hao Zhang, and Terence Darlington Mushore. 2018. "Spatiotemporal Analysis of Land Use/Land Cover and Its Effects on Surface Urban Heat Island Using Landsat Data: A Case Study of Metropolitan City Tehran (1988–2018)." *Sustainability (Switzerland)* 10 (12). 10.3390/su10124433.
- Roy, D.P., Wulder, M.A., Loveland, T.R., Woodcock, C.E., Allen, R.G., Anderson, M.C., Helder, D., Irons, J.R., Johnson, D.M., Kennedy, R., 2014. Landsat-8: Science and Product Vision for Terrestrial Global Change Research. *Remote Sens. Environ.* 145, 154–172.
- Sharma, A., Conry, P., Fernando, H.J.S., Hamlet, A.F., Hellmann, J.J., Chen, F., 2016. Green and Cool Roofs to Mitigate Urban Heat Island Effects in the Chicago Metropolitan Area: Evaluation with a Regional Climate Model. *Environ. Res. Lett.* 11 (6), 64004.
- Shen, Ping, Jing Zhang, and Zhenghua Su. 2011. "The Application of Remote Sensing in the Extraction of Urban land Use Changes." In *Procedia Environmental Sciences*, 10:1589–94. Elsevier B.V. 10.1016/j.proenv.2011.09.252.
- Tucker, C.J., 1979. Red and Photographic Infrared I, Linear Combinations for Monitoring Vegetation. *Remote Sens. Environ.* 8.

- Van der Werff, H., Van der Meer, F., 2016. Sentinel-2A MSI and Landsat 8 OLI Provide Data Continuity for Geological Remote Sensing. *Remote Sens. (Basel)* 8 (11), 883.
- Ward, K., Lauf, S., Kleinschmit, B., Endlicher, W., 2016. Heat Waves and Urban Heat Islands in Europe: A Review of Relevant Drivers. *Sci. Total Environ.* 569, 527–539.
- Zha, Y., Gao, J., Ni, S., 2003. Use of Normalized Difference Built-up Index in Automatically Mapping Urban Areas from TM Imagery. *Int. J. Remote Sens.* 24 (3), 583–594. <https://doi.org/10.1080/01431160304987>.
- Zhang, X., Estoque, R.C., Murayama, Y., Ranagalage, M., 2021. Capturing Urban Heat Island Formation in a Subtropical City of China Based on Landsat Images: Implications for Sustainable Urban Development. *Environ. Monit. Assess.* 193, 1–13.
- Zhao, H., Chen, X., 2005. Use of Normalized Difference Bareness Index in Quickly Mapping Bare Areas from TM/ETM+. *Int. Geosci. Remote Sens. Symposium (IGARSS)* 3 (August), 1666–2168. <https://doi.org/10.1109/igarss.2005.1526319>.
- Zhu, W., Lü, A., Jia, S., 2013. Estimation of Daily Maximum and Minimum Air Temperature Using MODIS Land Surface Temperature Products. *Remote Sens. Environ.* 130, 62–73.